CHEMISTRY OF MATERIALS

Article

pubs.acs.org/cm

Control over Memory Performance of Layer-by-Layer Assembled Metal Phthalocyanine Multilayers via Molecular-Level Manipulation

Bonkee Koo,[†] Hyunhee Baek,[†] and Jinhan Cho*[,†]

[†]Department of Chemical and Biological Engineering, Korea University, Anam-dong, Seongbuk-gu, Seoul 136-713, Korea

Supporting Information

ABSTRACT: We herein report on the nonvolatile memory properties of iron phthalocyanine multilayers prepared using an electrostatic layer-by-layer assembly method. Cationic poly(allylamine hydrochloride) (PAH) and anionic iron(III) phthalocyanine-4, 4′, 4″, 4‴-tetrasulfonic acid (Fe-TsPc) were alternately deposited onto quartz glass, indium tin oxide (ITO), or platinum-coated silicon substrates via electrostatic interactions. The electrochemical response of the PAH/Fe-TsPc, which was obtained from cyclic voltammograms (CV) in solution, indicated that redox reactions occurred at the phthalocyanine unit and at the metallic center. It was found that these redox reactions of the PAH/Fe-TsPc multilayer films in solution could be extended to resistive switching nonvolatile memory based on a charge trap/release mechanism in air. The PAH/Fe-TsPc multilayers sandwiched between the bottom (platinum) and top (Ag or tungsten) electrodes exhibited the characteristics of a resistive switching memory at a relatively low operating voltage of less than 2 V, with a switching speed of about 100 ns and an ON/OFF current ratio of ~10^3. Additionally, it is confirmed using kelvin probe force microscopy (KPFM) that the reversible resistance changes in the PAH/Fe-TsPc multilayers are mainly caused by the externally applied voltage as a result of the trapping and release of charges at redox sites within the Fe-TsPc. Furthermore, in the case where insulating layers of about 2 nm in thickness are inserted between adjacent Fe-TsPc layers, it is demonstrated that these devices can exhibit further improvements in memory performance (ON/OFF current ratio of ~10^6) and a lower power consumption in comparison with PAH/Fe-TsPc multilayers.

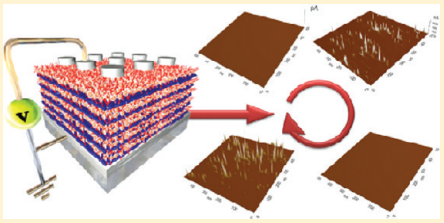

KEYWORDS: *iron-phthalocyanine, multilayers, layer-by-layer assembly, charge trap, nonvolatile memory*

INTRODUCTION

Nonvolatile resistive switching memory (NRSM) devices, which show rapid switching speeds of nanoseconds and a high ON/OFF current ratio of above ~10^2, have attracted considerable attention due to the widespread use of mobile electronics such as MP3 players, digital cameras, and mobile telephones.[1−10] In addition, these devices have a simple structure composed of a resistive material between two electron conductors, and they can operate without transistors in every cell. NRSM devices with high memory function and performance stability can be prepared from a variety of transition metal oxides such as TiO_x, ZrO_x, or NiO through vacuum deposition.[11,12] However, polymers with electrically induced responses have significant advantages over such transition metal oxide films in that the polymers can be used to produce low-cost devices through simplified solution processes, such as spin-coating.[13−18] Recently, it was reported that nonvolatile memory devices based on solution-processable organic materials exhibit relatively high ON/OFF current ratios of above 10^3 and have the write-once−read-many times (WORM) memory characteristics, without the ability to rewrite or change the voltage polarity after switching to the "ON state".[7,19,20] More recently, it was reported that organic memory devices with voltage polarity-dependent switching (i.e., bipolar resistive switching) and high memory performance could be prepared using an insulating organic matrix containing charge trap elements, such as graphene or inorganic nanoparticles.[21−23] However, these approaches may lead to aggregates with dimensions of several hundred nanometers due to thermodynamically unfavorable interactions when either the concentration of the functional components (i.e., inorganic nanoparticles or organic materials with a low M_w) inserted within the polymer matrix or the operating temperature is increased beyond a critical level.

The layer-by-layer assembly method, which is based on a solution dipping process, offers diverse opportunities to prepare nanocomposite films with functionalities and layer thicknesses that can be tailored at the nanoscale, in addition to the formation of a variety of desired components on substrates of different sizes and shapes.[24−36] Recently, we reported that (cationic polyelectrolyte (PE)/anionic titanium precursor)$_n$ multilayers prepared *via* electrostatic LbL assembly were converted into inorganic TiO_x films by thermal annealing at 450 °C, and the resultant films exhibited resistive switching characteristics that were independent of voltage polarity (i.e., unipolar resistive switching).[35] However, using our previous approach, which required thermal treatment at a high temperature, we had difficulty in creating memory cells on plastic substrates, such as poly(ethylene terephthalate) (PET).

Received: November 15, 2011
Revised: February 29, 2012
Published: March 5, 2012

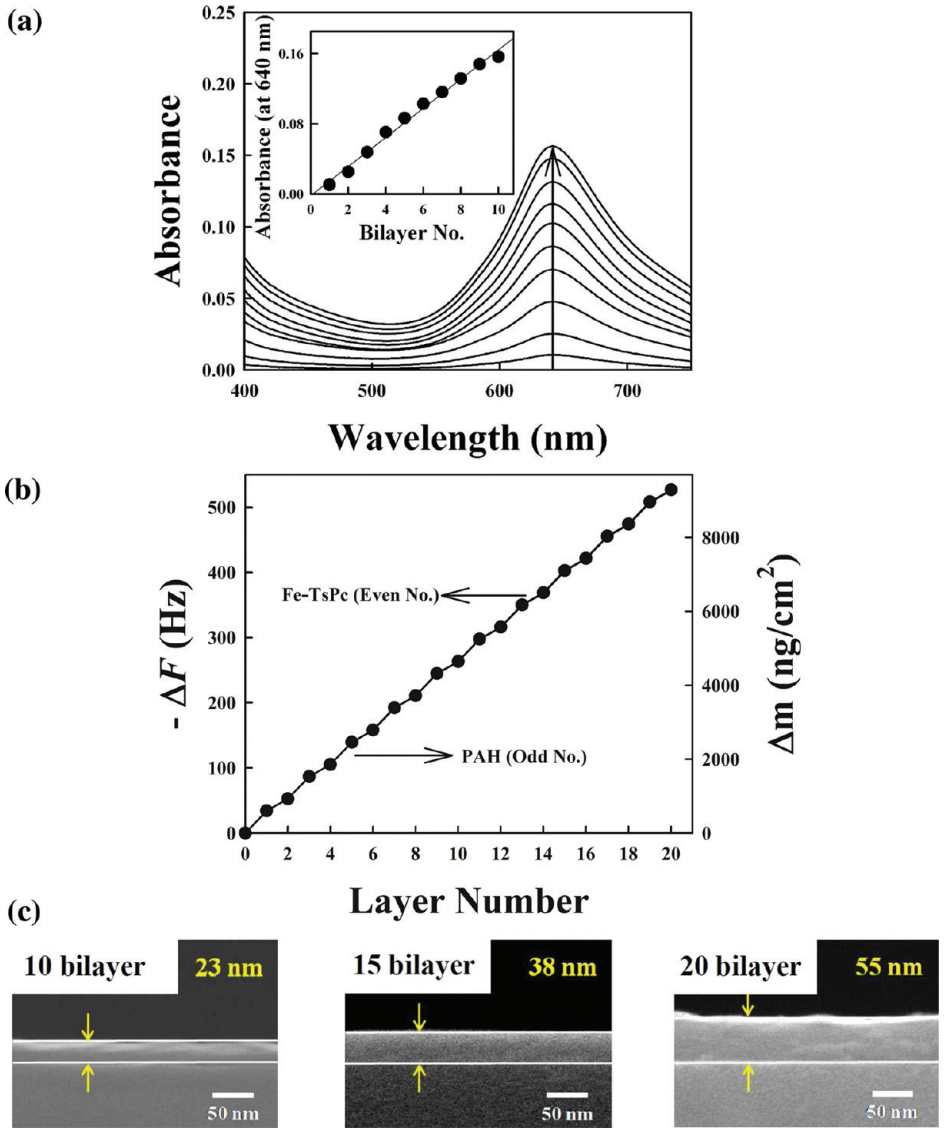

Figure 1. (a) UV−vis spectra of PAH/Fe-TsPc multilayers measured with an increasing number of bilayers ranging from 1 to 10. The inset indicates the linear increase of absorbance measured at a 640 nm wavelength as a function of bilayer number. (b) Frequency and mass change of PAH/Fe-TsPc multilayers measured with an increasing number of layers ranging from 1 to 20. (c) Cross-sectional SEM images of $(PAH/Fe\text{-}TsPc)_{n=10,\ 15\ and\ 20}$ multilayers.

Therefore, in order to incorporate the primary advantages of the LbL assembly method into nonvolatile memory devices, electrostatically charged organic materials possessing resistive switching properties that do not require high temperature treatments should be used, and the amounts and thicknesses of the adsorbed material should be quantified at the nanoscale. Additionally, the resulting film devices should possess detectable changes between the different resistance states, while still possessing relatively low operating voltages and fast switching speeds.

In this study, LbL-assembled cationic poly(allylamine hydrochloride) (PAH))/anionic iron(III) phthalocyanine-4, 4,′ 4″, 4‴-tetrasulfonic acid (Fe-TsPc) multilayers were deposited onto a platinum (Pt) electrode in order to prepare nanocomposite film devices with tailored nanostructures and resistive switching properties. Although it was reported by the Advincula group that organic thin film transistors could be successfully prepared from LbL-assembled multilayer films composed of copper phthalocyanine layers, our approach focused on resistive switching nonvolatile memory cells instead of transistor-type devices.[36] The LbL-assembled $(PAH/Fe\text{-}TsPc)_n$ devices exhibited a bipolar resistive switching behavior that facilitated repeated writing and erasing at low operating voltages of less than 2 V and a rapid switching speed of 100 ns in air. Additionally, we used Kelvin probe force microscopy (KPFM) to demonstrate that the switching mechanism of the PAH/Fe-TsPc multilayer devices mainly originated from charge trapping and release within the redox sites of the Fe-TsPc. Our study is significant because a variety of metallophthalocyanines that possess redox sites can be used as the active resistive switching layer. Furthermore, our approach, which is based on LbL-assembled metallophthalocyanine multilayers, is effective for the preparation of large-area memory devices at room temperature.

■ EXPERIMENTAL SECTION

Preparation of the Multilayers. We used solutions of iron(III) phthalocyanine-4, 4′, 4″, 4‴-tetrasulfonic acid with oxygen mono-

dx.doi.org/10.1021/cm2033959 | Chem. Mater. 2012, 24, 1091−1099

sodium salt hydrate (M_w = 947, Fe-TsPc, Aldrich), poly(allylamine hydrochloride) (PAH) (M_w = 70 000, Aldrich), poly(acrylic acid) (PAA) (M_w = 1800, Aldrich), poly(4-sodium, styrenesulfonic acid) (PSS) (M_w = 70 000, Aldrich) with concentrations of 0.5, 1, 1, and 1 mg·mL^{-1} for all of our experiments. The pH of the cationic PAH and anionic Fe-TsPc solutions was adjusted to 5 using 0.1 M NaOH (for PAH) and HCl (for Fe-TsPc), respectively. Pt-coated Si substrates (for the preparation of nonvolatile memory devices) were irradiated with UV light to create an anionic surface. On the other hand, the surfaces of quartz (for the measurements of UV−vis spectroscopy) and indium tin oxide (ITO) glasses (for the measurements of cyclic voltammograms) were negatively charged by heating at 70 °C for 20 min in a 5:1:1 vol % mixture of water, hydrogen peroxide, and 29% ammonia solution (RCA solution). After surface treatment, these substrates were dipped into the cationic PAH solution for 10 min, washed twice by dipping in water for 1 min, and spin-dried at a speed of 4000 rpm for 30 s using a spin-coater (YA-101, Yooil Engineering). Anionic Fe-TsPc was subsequently deposited onto the PAH-coated substrates using the same adsorption, washing, and drying procedures as those described above. This process was repeated until the desired number of layers was deposited. The resultant multilayer films were thermally annealed at 80 °C for 2 h under air.

Quartz Crystal Microgravimetry (QCM) Measurements. A QCM device (QCM200, SRS) was used to investigate the mass of material deposited after each adsorption step. The resonance frequency of the QCM electrodes was ca. 5 MHz. All the processes for PAH/Fe-TsPc multilayer deposition onto QCM electrodes exactly coincided with those performed on Pt-coated Si substrates. The adsorbed masses of PAH and Fe-TsPc, Δm, can be calculated from the change in the frequency of the QCM electrodes, ΔF, according to the Sauerbrey equation: ΔF (Hz) = $-56.6 \times \Delta m_A$, where Δm_A is the mass change per quartz crystal unit area in μg·cm^{-2}.

Surface Morphology. The surface morphology and roughness of the Fe-TsPc-based multilayers on the Si substrates were measured with an atomic force microscope (AFM) in the tapping mode (SPA400, SEIKO).

Cyclic Voltammetry (CV) Measurements. Electrochemical activities of multilayers adsorbed onto ITO electrodes were investigated by using cyclic voltammetry (CV) (Compactstat, IVIUM). In this case, CV curves of multilayer-coated ITO electrodes were measured in 0.1 M HCl as a function of the scan rate.

UV−vis Spectrophotometry. UV−vis spectra of PAH/Fe-TsPc multilayers on negatively charged quartz glass were taken with a Perkin-Elmer Lambda 35 UV−vis spectrometer. The electronic absorption of the Fe-TsPc monomeric species shows an absorbance band centered at 640 nm.

Fourier Transform Infrared Spectroscopy (FTIR). Vibrational spectroscopic characterization was carried out using FTIR spectroscopy (spectrum 400, Perkin-Elmer) in the transmission and attenuated total reflection (ATR) modes. The sample chamber was purged with N_2 gas for 2 h to eliminate water and CO_2 before FTIR measurement. An ATR-FTIR spectrum for the $(PAH/Fe\text{-}TsPc)_{20}$ film deposited onto an Au-coated substrate was obtained from 300 scans with an incident angle of 80°.

X-ray Photoelectron Spectroscopy (XPS). Fe ions within PAH/Fe-TsPc multilayers were analyzed by using XPS equipment (Sigma Probe, ThermoVG, Hove, U.K.). The XPS spectra were acquired using a monochromatic A-K source (100 W).

Fabrication of Resistive Switching Memory Devices. All of the samples were prepared on Si substrates (2 cm × 2 cm) with a 100-nm-thick SiO_2 layer. A 20-nm-thick Ti layer was subsequently deposited on the substrates, and the bottom electrode (Pt) was deposited using a DC-magnetron sputtering system. Next, the $(PAH/Fe\text{-}TsPc)_n$ multilayer films were formed on the Pt-coated Si substrates. The resultant multilayer films were thermally annealed at 80 °C for 2 h in air. After thermal conversion, top electrodes of 100 μm in diameter were deposited onto the nanocomposite films. To investigate the resistive switching behavior of LbL assembled multilayered devices, current−voltage (I−V) curves were measured on a semiconductor parametric analyzer (SPA, Agilent 4155B) in air. The dependence of the high and low current states on the voltage pulse duration was investigated using a semiconductor parametric analyzer (HP 4155A) and a pulse generator (Agilent 81104A). *Although Ag electrodes were used as the top electrodes in these devices, similar switching behavior was also observed when using Au, Pt, or W top electrodes. This finding indicates that the Ag electrode itself has no significant effect on the resistive switching characteristics of the LbL $(PAH/Fe\text{-}TsPc)_n$ multilayers.*

RESULTS AND DISCUSSION

The electrostatic LbL assembly of cationic PAH and anionic Fe-TsPc, both with a pH of 5, was first performed on quartz glass substrates for UV−vis spectroscopy, as shown in Figure 1a. The absorbance at 640 nm (Q-band of phthalocyanine) corresponds to the electronic absorption of the Fe-TsPc monomeric species.[37−39] The uniform growth of the absorbance at 641 nm indicates that the adsorbed amount of Fe-TsPc per bilayer is consistent, demonstrating the uniform growth of PAH/Fe-TsPc multilayers (the inset of Figure 1a). The amount of PAH and Fe-TsPc adsorbed on the multilayer films was quantified by quartz crystal microgravimetry (QCM) (Figure 1b). Measuring the frequency changes from which the mass changes were calculated for the alternating deposition of PAH and Fe-TsPc gave a $-\Delta F$ of 34 ± 3 Hz (Δm of ∼601 ng·cm^{-2}) and 19 ± 2 Hz (Δm of ∼329 ng·cm^{-2} and a number density of Fe ions ∼2.14 × 10^{14}·cm^{-2}), respectively. The formation of $(PAH/Fe\text{-}TsPc)_n$ multilayers was further characterized by scanning electron microscopy (SEM) (Figure 1c). The total thicknesses of the $(PAH/Fe\text{-}TsPc)_n$ multilayer films were measured as a function of bilayer number and were found to be approximately 23 nm for n = 10, 38 nm for n = 15, and 55 nm for n = 20 (Figure 1c; Supporting Information, Figure S1). The root-mean-surface (rms) roughness of $(PAH/Fe\text{-}TsPc)_{20}$ multilayer films was measured to be about 1 nm (see Supporting Information, Figure S2). Although it was reported that the development of PAH/Fe-TsPc multilayers was partially assisted by complementary interactions between the nitrogen atom of the unprotonated amino group and the coordinating metal of the phthalocyanine,[40] the interactions that formed in our study were governed only by electrostatic interactions, as the amino groups of the PAH are fully protonated at a pH of 5.[41]

We also investigated the vibrational spectroscopic properties of LbL-assembled PAH/Fe-TsPc multilayer films using the transmission and ATR modes of FTIR. As shown in Figure 2, the main bands of PAH are assigned wavenumbers in cm^{-1} of 1525, 1595 (N−H bending), and 1350 (C−H bending). The Fe-TsPc cast film displayed the following main absorption bands: 770 (ring breathing, C−H wagging), 1030 (SO_3 stretching), 1200 (SO_3 stretching), and 1625 cm^{-1} (C═C benzene stretching). The band at 1030 cm^{-1} due to the SO_3 stretching in spectrum b appears as a stronger band shifted to 1025 cm^{-1} in the LbL-assembled PAH/Fe-TsPc film spectrum c. Additionally, the band at 1200 cm^{-1} (SO_3 stretching) splits into two bands at 1190 and 1223 cm^{-1} with an increase in relative intensity in the LbL films compared to the neat Fe-TsPc film. These phenomena occurred due to the formation of electrostatic bonding between SO_3^- of Fe-TsPc and NH_3^+ of PAH in the LbL films. It was reported that Fe-TsPc molecules in the LbL-assembled PAH/Fe-TsPc multilayer films were perpendicular to the substrate plane based on the ATR-FTIR results that the band of phthalocyanine at 1123 cm^{-1} assigned to in-plane C−H bending dominated the ATR-FTIR spectrum for the LbL film, whereas it vanished in the transmission

dx.doi.org/10.1021/cm2033959 | Chem. Mater. 2012, 24, 1091−1099

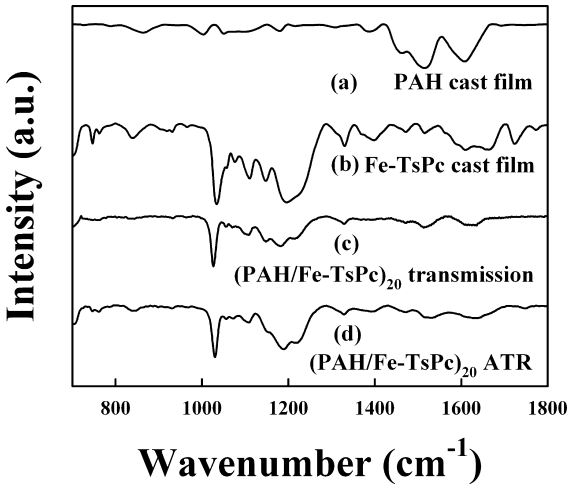

Figure 2. FTIR spectra for (a) neat PAH and (b) Fe-TsPc and for LbL films of (c) $(PAH/Fe\text{-}TsPc)_{20}$ onto Si (transmission mode) and (d) onto Au (attenuated total reflection [ATR] mode).

mode.[40] However, we did not observe any notable difference between the transmission-FTIR and ATR-FTIR spectra of LbL-assembled PAH/Fe-TsPc films. That is, the evident absorption band at 1123 cm^{-1} was not shown in the ATR-FTIR spectrum. These results indicate that the adsorbed Fe-TsPc molecules are preferentially aligned with the substrate plane.

The spectral shape and the binding energies of the significant peaks for Fe $2p_{3/2}$ (708.6 eV) and Fe $2p_{1/2}$ (723.6 eV) in the X-ray photoelectron spectroscopy (XPS) pattern of the PAH/Fe-TsPc multilayers were derived from the Fe ions within the Fe-TsPc layers (Figure 3a).[42] Additionally, these Fe ions give rise to the electrochemical properties of PAH/Fe-TsPc multilayers through the Fe^{III}/Fe^{II} redox reaction, which is induced by the voltage applied to the solution. Figure 3b depicts the cyclic voltammograms for PAH/Fe-TsPc multilayers at various scan rates, exhibiting two redox reactions at E_a (i.e., E_{Oa} and E_{Ra}) and E_b (i.e., E_{Ob} and E_{Rb}). These redox reactions were attributed to the phthalocyanine ring and the Fe^{III}/Fe^{II} couple, respectively. Alencar et al. reported that the first, slower, oxidation process occurs in the phthalocyanine unit (E_{Oa}), whereas the second, faster, oxidation occurs at the Fe^{II} metallic center (E_{Ob}).[39] The subsequent, faster, reduction (E_{Rb}) occurs at the Fe^{III} sites, whereas the second, slower, reduction occurs at the phthalocyanine unit (E_{Ra}). They also reported that the second oxidation process, which is attributed to the Fe^{III}/Fe^{II}, occurs at higher potentials than those for other metal-lophthalocyanines such as Ni-TsPc. As shown in Figure 3c and 3d, the cathodic and anodic peak currents for the PAH/Fe-TsPc multilayers linearly increase with the scan rate, indicating that the electrochemical response is governed by a charge-transfer mechanism.[39] In addition, PAH/Fe-TsPc multilayer systems display similar characteristics to redox polymer systems, wherein charge transport within the multilayers is

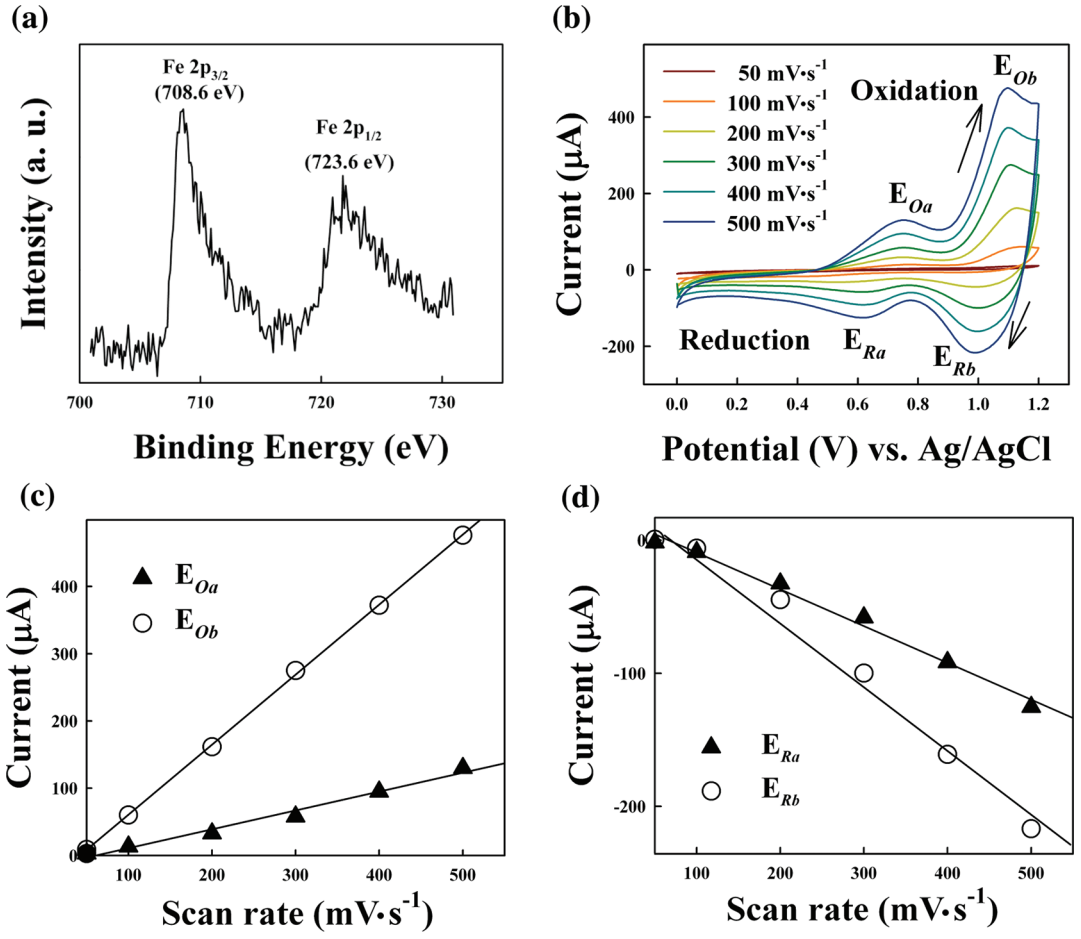

Figure 3. (a) XPS spectrum of LbL-assembled PAH/Fe-TsPc multilayers. (b) Cyclic voltammogram of a $(PAH/Fe\text{-}TsPc)_{20}$ multilayer-coated ITO electrode in 0.1 M HCl as a function of scan rate. Scan rate dependence of (c) cathodic (E_{Oa}) and (d) anodic peak currents (E_{Ra}).

dx.doi.org/10.1021/cm2033959 | *Chem. Mater.* 2012, 24, 1091–1099

Scheme 1. Schematics for the Setup of the PAH/Fe-PC Multilayer-Based Nonvolatile Memory Devices

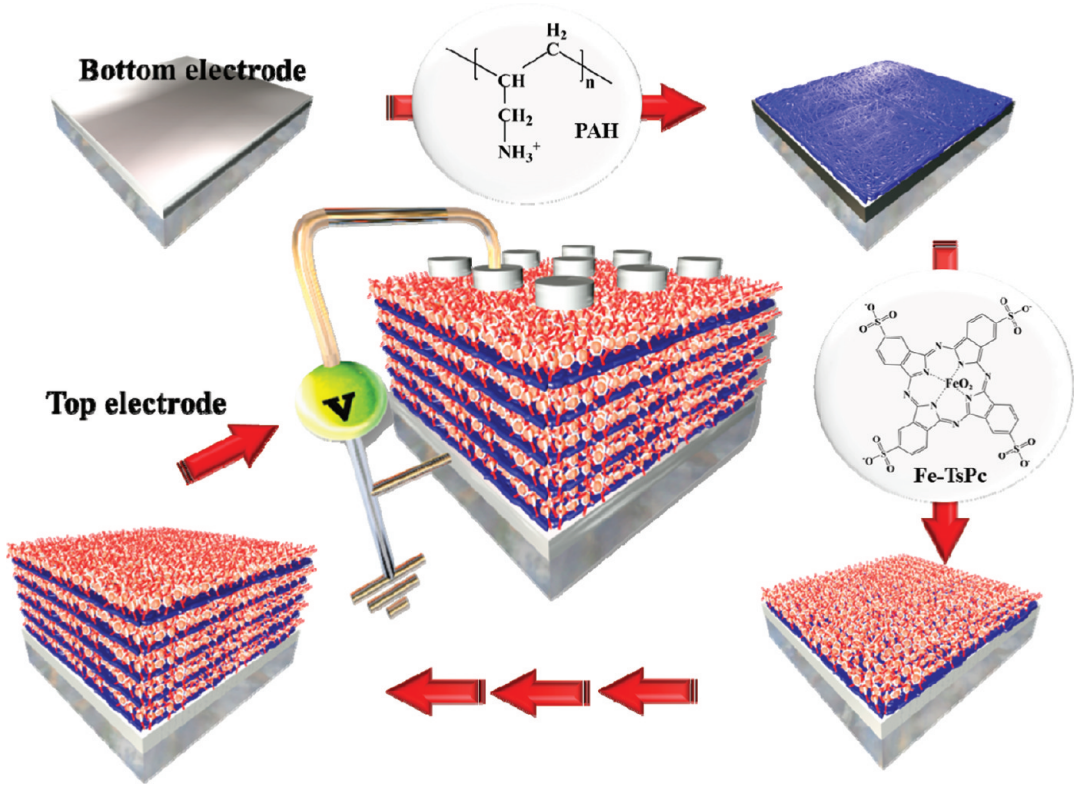

expected to occur via electron hopping, which is consistent with the findings of Laurent and Schlenoff.[34,38] Considering that these redox reactions are closely related to electron release (oxidation) and trapping (reduction), PAH/Fe-TsPc films may possess resistance-switching properties, which cause a reversible change in resistance based on an externally applied voltage.

Based on this possibility, devices composed of a Pt bottom electrode, $(PAH/Fe\text{-}TsPc)_n$ multilayers, and an Ag top electrode were prepared with electrode diameters of 100 μm and an increase in the number of bilayers, as illustrated in Scheme 1.

In order to examine the bistable switching behavior of these multilayered devices, an initial negative bias sweep from 0 to −1.8 V with a current limit of 100 mA was applied (Figure 4a). For these devices, the current abruptly increases at −1.6 V (which we define as V_{SET}) and causes the device to transition from an insulating state (i.e., "OFF" state) to a conductive state (i.e., "ON" state). When the reverse voltage polarity was applied to the $(PAH/Fe\text{-}TsPc)_{20}$ multilayer devices, this high-current state was maintained at up to +1.5 V (which we define here as V_{RESET}), which induced a sudden decrease in current. The current of the OFF state increases inversely with the voltage. At a proper reading voltage (e.g., ± 0.1 V), the current ratio between high and low conductivity is greater than 10^2, which is a large enough difference to detect the different states. In addition, decreasing the number of bilayers (i.e., decreased multilayer thickness) increases the OFF current level because decreases in film thickness increase the electric field strength. Figure 4b depicts the results of cycling tests with a switching speed of 100 ns for PAH/Fe-TsPc film devices with 20 bilayers. More than 200 SET/RESET cycles have been demonstrated without a loss of sensitivity. Furthermore, the retention times of the $(PAH/Fe\text{-}TsPc)_{20}$ multilayered devices were tested to determine the electrical stability of the ON and OFF states when using a reading voltage of +0.1 V, and the ON and OFF states were found to be stable in air for a period above 10^5 s (Figure 4c).

In order to understand the conduction mechanism of the PAH/Fe-TsPc multilayers, the $I-V$ characteristics in the negative voltage sweep region of films containing 20 bilayers were plotted and fitted on a log−log scale (Figure 4d). The $I-V$ relationship in the ON state clearly exhibits ohmic conductance behavior with a slope of ~1.0, which indicates the formation of conductive pathways in the device during the SET process; however, the conduction behavior of the films in the OFF state was more complicated. The results for the charge transport behavior of the high-resistance state are consistent with trap-controlled space charge−limited conduction (SCLC).[43,44] This conduction consists of three different conductivity regions: the ohmic region ($I \propto V$) at a low negative voltage, a transition region ($I \propto V^2$) that spans from the ohmic region to the SCLC transport, and a region in which there is a sharp current increase. The different conduction behaviors in the ON and OFF states imply that the ON/OFF switching of the Fe-TsPc-based memory devices is governed by SCLC and localized filament mechanisms.

The formation of localized conductive filamentary pathways was also confirmed using current-sensing AFM (CS-AFM) using an electrochemically inert Pt tip instead of Ag as the top electrode (Figure 5). Formation and rupture of randomly distributed pathways were observed after the "SET" (i.e., switching from low current, OFF to high current, ON state) and "RESET" (i.e., switching from high current, ON to low current, OFF state) processes, respectively. This finding suggests that the current density was not uniform between the top and bottom electrodes but was concentrated in these

dx.doi.org/10.1021/cm2033959 | *Chem. Mater.* 2012, 24, 1091−1099

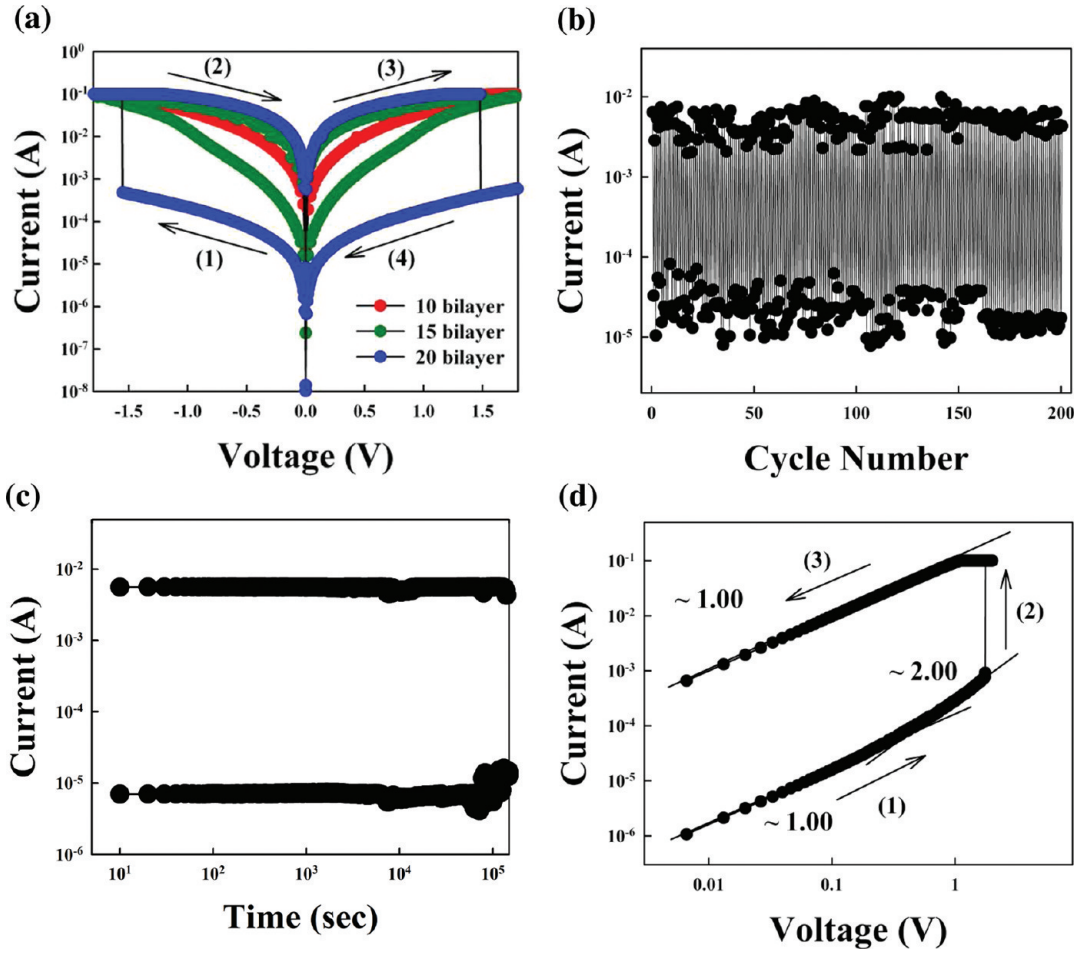

Figure 4. (a) $I-V$ curves of $(PAH/Fe\text{-}TsPc)_n$ multilayer devices with an increasing number of bilayers (n), ranging from 10 to 20. (b) The cycling and (c) retention tests of a device with 20 bilayers that was measured to have a switching speed of 100 ns. (d) The linear fitting for the $I-V$ curve.

localized conducting pathways, which are turned on and off during switching.[46] Considering that the electron transport in organic materials with transition metal complexes is mainly caused by an electron-hopping process, these conductive paths are formed by electron hopping between charge trap sites.

Although the switching mechanism of NRSM devices based on transition metal oxide can be adequately explained by either the memristor model (for bipolar switching characteristics)[2,3,11,46] or the filamentary conduction model (for unipolar switching characteristic),[48] the bipolar switching behavior in our samples may be due to charge storage (high resistance) and release (low resistance) within charge-trap sites according to the Simmons-Verderber model.[48−52] In the PAH/Fe-TsPc multilayered film devices, the electrically active sites with Fe^{III}/Fe^{II} redox couples can be used as charge trap elements, which can considerably affect the switching mechanisms of devices. First, a negative voltage sweep from 0 to −1.8 V stores electrons within the redox sites and induces a low conductive state (i.e., region (1) in Figure 3a). This OFF state is maintained until the electrons are released from the redox sites. At the SET (switching from low current, OFF to high current, ON state) voltage of −1.6 V, the current suddenly increased, implying the formation of conductive pathways based on the release of electrons from the redox sites. This highly conductive state (i.e., (2) → (3)) is maintained during reverse voltage sweeps from −1.8 to +1.5 V; however, the subsequent reversal of the voltage polarity breaks down the conductive paths for the electrons in the Fe-TsPc multilayers, resulting in a decrease in conductivity corresponding to the RESET process (i.e., switching from the ON to the OFF state). These phenomena were also confirmed using a variety of metallophthalocyanine (i.e., Ni-TsPc and Cu-TsPc)-based multilayers (see Supporting Information, Figure S3); however, we cannot exclude the possibility that charge-trap and -release processes can also occur in the phthalocyanine unit in addition to the metallic center, because the redox reaction of phthalocyanine was observed in the cyclic voltammograms for the PAH/Fe-TsPc multilayer-coated electrode, as shown in Figure 3b.

To prove that the switching mechanism was being shown in the PAH/Fe-TsPc multilayered film devices, we examined the changes in the real-space imaging of the charge trap and release states using KPFM (Figure 6). The charges stored within the Fe-TsPc could be detected by observing the change in the surface potential when the tip (i.e., a 20-nm-diameter Au-coated tip) of the KPFM scanned the surface of the PAH/Fe-TsPc multilayers. First, a 12 × 12 μm^2 area of the multilayer film was scanned for charge traps at +12 V and at −12 V over a 9 × 9 μm^2 area for charge releases. Next, the operation was performed again, scanning a 5 × 5 μm^2 area at +12 V for charge traps and a 2 × 2 μm^2 area at −12 V for charge releases. As displayed in Figure 5, the yellow region indicates a charge trapped state and the dark region corresponds to the charge released state. These results show that nonvolatile devices

dx.doi.org/10.1021/cm2033959 | Chem. Mater. 2012, 24, 1091−1099

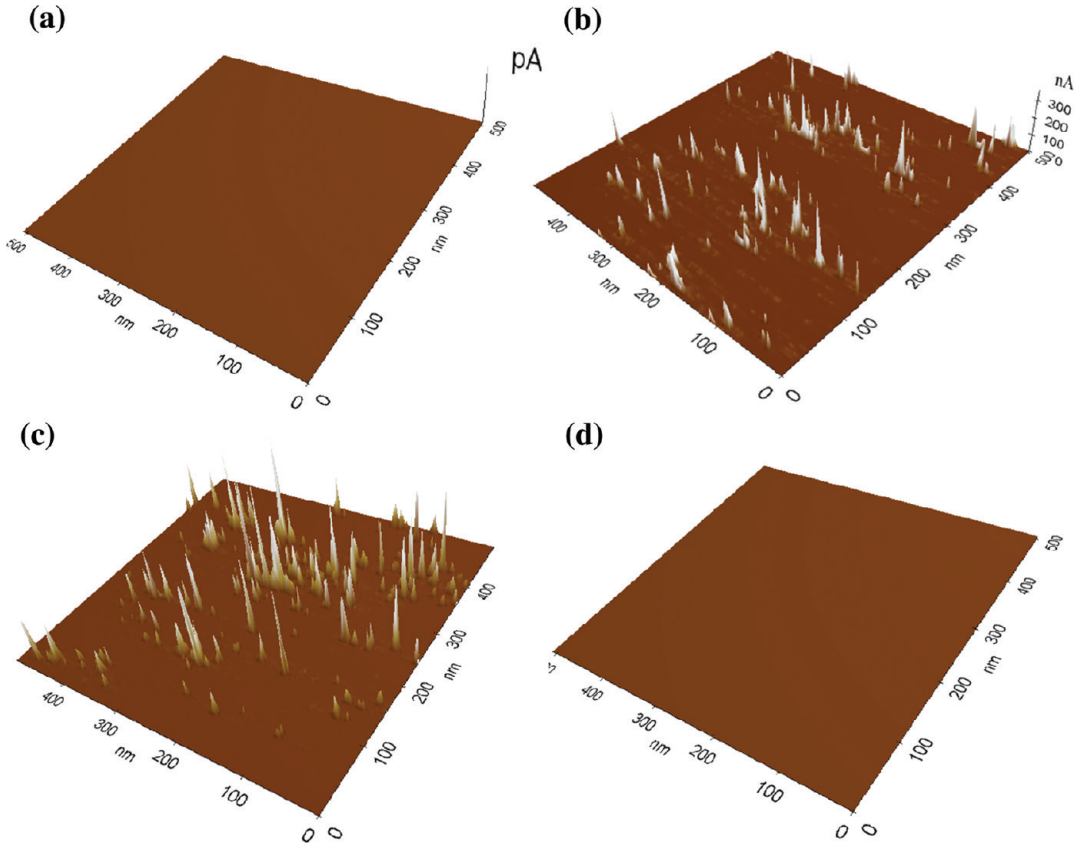

Figure 5. CS-AFM images of the PAH/Fe-TsPc multilayers for the charge trap/release operations. It was observed that the number of conductive filaments sharply grew with the applied voltage. (a) 0 V, (b) 1.5 V, (c) 1.5 V, and (d) 0 V.

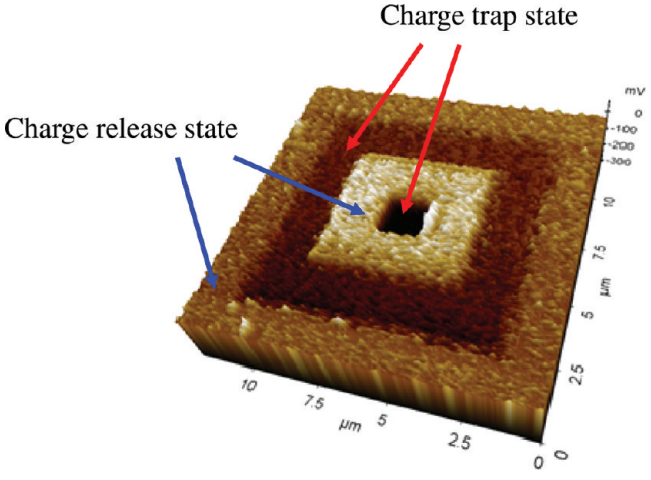

Figure 6. KPFM images of the PAH/Fe-TsPc multilayers for the charge trap/release operations.

composed of PAH/Fe-TsPc multilayers operate through a charge trap and release mechanism.

Based on these results, we have tried to significantly improve the memory performance of Fe-TsPc multilayer devices by molecular-level manipulation. Our motivation was based on the possibility that the further insertion of insulating layers of about 2 nm in thickness between electrically active Fe-TsPc layers could effectively screen the leakage current in the ON and OFF current states and consequently induce low power consumption. For this investigation, (PAH/Fe-TsPc/PAH/anioic poly(acrylic acid) (PAA))$_{10}$ multilayers were used instead of (PAH/Fe-TsPc)$_{20}$ multilayers (Figure 7). In this case, the (PAH/Fe-TsPc/PAH/PAA)$_{10}$ multilayer device exhibited a higher ON/OFF current ratio of ~10^6 and a lower current level (ON current level of 10^{-5} A and OFF current of 10^{-11}A at a reading voltage of −0.1 V) than those (ON/OFF current ratio ~10^3, ON current level of 10^{-2} and OFF current level of 10^{-5} A at a reading voltage of −0.1 V) of the (PAH/Fe-TsPc)$_{15}$ multilayer device. On the other hand, the operating voltages of these devices were not significantly increased compared to those of PAH/Fe-TsPc multilayered devices. That is, the charge carriers

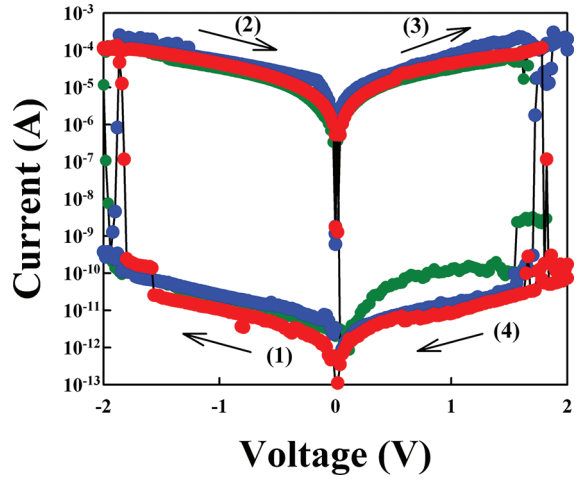

Figure 7. $I-V$ curves of (PAH/Fe-TsPc/PAH/PAA)$_{10}$ multilayer devices.

dx.doi.org/10.1021/cm2033959 | *Chem. Mater.* 2012, 24, 1091−1099

(i.e., electrons) captured within the Fe-TsPc in the (PAH/Fe-TsPc/PAH/PAA)$_{10}$ multilayers generate enough internal field to form conducting filamentary paths across the inserted insulating layers, and as a result these devices exhibited decreased leakage current flow, although the PAH/PAA film devices without Fe-TsPc layers cannot possess the memory effect. On the other hand, in the case of inserting anionic poly(4-sodium, styrenesulfonic acid) (PSS) into Fe-TsPc-based multilayers instead of PAA (i.e., (PAH/Fe-TsPc/PAH/PSS)$_{10}$ multilayer), these devices exhibited a relatively low ON/OFF current ratio of ~10^3 due to the increase of leakage current in the OFF current level compared to that of the (PAH/Fe-TsPc/PAH/PAA)$_{10}$ multilayer device (see Supporting Information, Figure S4). It was reported by the Rubner group that the strong sulfonic acid groups of PSS could promote the electrochemical oxidation (i.e., an increase of current level) of the multilayer films, and this "polyanion-type doping" would not be expected from the use of the weak carboxylic acid groups of PAA.[53] As a result, this molecular-level control over device architecture via the use of the LbL assembly approach makes it possible to access the thickness regime and modulate the electrical properties, which is simply not possible with conventional processing techniques.

CONCLUSIONS

We have demonstrated that LbL-assembled PAH/Fe-TsPc multilayer films can be used as the electrically active layers of NRSM devices and that their memory performance can be significantly enhanced by an additional insertion of insulating layers between adjacent Fe-TsPc layers. The formed devices exhibited voltage polarity-dependent switching properties with a high ON/OFF current ratio of more than 10^6 and a low current flow at relatively low operating voltages (i.e., V_{RESET} ~ +1.5 V and V_{SET} ~ −1.6 V). These phenomena were primarily caused by the trapping and releasing of charges at the redox sites (i.e., metallic center and phthalocyanine ring) within the Fe-TsPc. The importance of this study is that metal-lophthalocyanine allows a variety of transition metal ions (i.e., charge trap elements) to be easily incorporated into the LbL-assembled multilayers and, furthermore, allows us to design large-area nonvolatile memory devices with adjustable memory performance *via* molecular level manipulation.

ASSOCIATED CONTENT

Supporting Information

Film thickness, AFM image, and *I*−*V* curves of multilayer films. This material is available free of charge via the Internet at http://pubs.acs.org.

AUTHOR INFORMATION

Corresponding Author

*E-mail: jinhan71@korea.ac.kr.

Notes

The authors declare no competing financial interest.

ACKNOWLEDGMENTS

This work was supported by KOSEF grant funded by the Korea government (MEST) (2010-0029106; 2010-00027751; R11-2005-048-00000-0).

REFERENCES

(1) Waser, R.; Aono, M. *Nat. Mater.* **2007**, *6*, 833−840.
(2) Strukov, D. B.; Snider, G. S.; Stewart, D. R.; Williams, R. S. *Nature* **2008**, *453*, 80−83.
(3) Yang, J. J.; Pickett, M. D.; Li, X.; Ohlberg, D. A. A.; Stewart, D. R.; Williams, R. S. *Nat. Nanotech.* **2008**, *3*, 429−433.
(4) Zhang, T.; Su, Z.; Chen, H.; Ding, L.; Zhang, W. *Appl. Phys. Lett.* **2008**, *93*, 172104−172104.
(5) Kim., Y.; Lee, C.; Shim, I.; Wang, D.; Cho, J. *Adv. Mater.* **2010**, *222*, 5140−5144.
(6) Bozano, L. D.; Kean, B. W.; Beinhoff, M.; Carter, K. R.; Rice, P. M.; Scott, J. C. *Adv. Funct. Mater.* **2005**, *15*, 1933−1939.
(7) Choi, S.; Hong, S.-H.; Cho, S. H.; Park, S.; Park, S.-M.; Kim, O.; Ree, M. *Adv. Mater.* **2008**, *20*, 1766−1771.
(8) Ji, Y.; Cho, B.; Song, S.; Kim, T.-W.; Choe, M.; Kahng, Y. H.; Lee, T. *Adv. Mater.* **2010**, *22*, 3071−3075.
(9) Heremans, P.; Gelinck, G. H.; Muller, R.; Baeg, K.-J.; Kim, D.-Y.; Noh, Y.-Y. *Chem. Mater.* **2011**, *23*, 341−358.
(10) Li, G. L.; Liu, G.; Li, M.; Wan, D.; Neoh, K. G.; Kang, E. T. *J. Phys. Chem. C* **2010**, *114*, 12742−12748.
(11) Yang, J. J.; Strachan, J. P.; Xia, Q.; Ohlberg, D. A. A.; Kuekes, P. J.; Kelley, R. D.; Stickle, W. F.; Stewart, D. R.; Medeiros-Ribeiro, G.; Williams, R. S. *Adv. Mater.* **2010**, *22*, 4034−4038.
(12) Nagashima, K.; Yanagida, T.; Oka, K.; Kanai, M.; Klamchuen, A.; Kim, J.-S.; Park, B.-H.; Kawai, T. *Nano Lett.* **2011**, *11*, 2114−2118.
(13) Liu, Z.; Yasseri, A. A.; Lindsey, J. S.; Bocian, D. F. *Science* **2003**, *302*, 1543−1544.
(14) Barman, S.; Deng, F.; McCreery, R. L. *J. Am. Chem. Soc.* **2008**, *130*, 11073−11081.
(15) Choi, S.; Hong, S.-H.; Cho, S. H.; Park, S.; Park, S.-M.; Kim, O.; Ree, M. *Adv. Mater.* **2008**, *20*, 1766−1771.
(16) Medalsy, I.; Klein, M.; Heyman, A.; Shoseyov, O.; Remacle, F.; Levine, R. D.; Porath, D. *Nat. Nanotech.* **2010**, *5*, 451−457.
(17) Ruiter, G. D.; Boom, M. E. V. D. *ACC. Chem. Res.* **2011**, *44*, 563−573.
(18) Simão, C.; Mas-Torrent, M.; Crivillers, N.; Lloveras, V.; Artěs, J. M.; Gorostiza, P.; Veciana, J.; Rovira, C. *Nat. Chem.* **2011**, *3*, 359−364.
(19) Lim, S. L.; Ling, Q.; Teo, E. Y. H.; Zhu, C. X.; Chan, D. S. H.; Kang, E.-T.; Neoh, K. G. *Chem. Mater.* **2007**, *19*, 5148−5157.
(20) Lee, T. J.; Park, S.; Hahm, S. G.; Kim, D. M.; Kim, K.; Kim, J.; Kwon, W.; Kim, Y.; Chang, T.; Lee, M. *J. Phys. Chem. C* **2009**, *113*, 3855−3861.
(21) Ouyang, J.; Chu, C.-W.; Szmanda, C. R.; Ma, L.; Yang, Y. *Nat. Mater.* **2004**, *3*, 918−922.
(22) Son, D. I.; Kim, T. W.; Sjim, J. H.; Jung, J. H.; Lee, D. U.; Lee, J. M.; Park, W. I.; Choi, W. K. *Nano Lett.* **2010**, *10*, 2441−2447.
(23) Son, D. I.; Park, D. H.; Kim, J. B.; Choi, J.-W.; Kim, T. W.; Angadi, B.; Yi, Y.; Choi, W. K. *J. Phys. Chem. C* **2011**, *115*, 2341−2348.
(24) Decher, G. Fuzzy *Science* **1997**, *277*, 1232−1237.
(25) Caruso, F.; Caruso, R. A.; Möhwald, H. *Science* **1998**, *282*, 1111−1114.
(26) Podsiadlo, P.; Kaushik, A. K.; Arruda, E. M.; Waas, A. M.; Shim, B. S.; Xu, J. D.; Nandivada, H.; Pumplin, B. G.; Lahann, J.; Ramamoorthy, A.; Kotov, N. A. *Science* **2007**, *318*, 80−83.
(27) Lee, B.; Kim, Y.; Lee, S.; Kim, Y. S.; Wang, D.; Cho, J. *Angew. Chem., Int. Ed.* **2010**, *49*, 359−363.
(28) Lee, J.-S.; Cho, J.; Lee, C.; Kim, I.; Park, J.; Kim, Y.; Shin, H.; Lee, J.; Caruso, F. *Nat. Nanotech.* **2007**, *2*, 790−795.
(29) Hong, J.; Bae, W.; Oh, S.; Lee, H.; Char, K.; Caruso, F.; Cho, J. *Adv. Mater.* **2007**, *19*, 4364−4369.
(30) Park, J.; Kim, I.; Shin, H.; Kim, Y. S.; Bang, J.; Caruso, F.; Cho, J. *Adv. Mater.* **2008**, *20*, 1843−1848.
(31) Cho, J.; Hong, J; Char, K.; Caruso, F. *J. Am. Chem. Soc.* **2006**, *128*, 9935−9942.
(32) Yoon, M.; Kim, Y.; Cho, J. *ACS Nano* **2011**, *5*, 5417−5426.
(33) Kim, S.; Kim, Y.; Ko, Y.; Cho, J. *J. Mater. Chem.* **2011**, *21*, 8008−8013.
(34) Kim, S.; Park, J.; Cho, J. *Nanotechnology* **2010**, *21*, 375702.
(35) Lee, C.; Kim, I.; Shin, H.; Kim, S.; Cho, J. *Langmuir* **2009**, *25*, 11276−11281.

(36) Locklin, J.; Shinbo, K.; Onishi, K.; Kaneko, F.; Bao, Z.; Advincula, R. C. *Chem. Mater.* **2003**, *15*, 1404−1412.
(37) Zhao, S.; Li, X.; Yang, M.; Sun, C. *J. Mater. Chem.* **2004**, *14*, 840−844.
(38) Alessio, P.; Rodriguez-Mendez, M. L.; Saez, J. A. D. S.; Constantino, C. J. L. *Phys. Chem. Chem. Phys.* **2010**, *12*, 3972−3983.
(39) Alencar, W. S.; Crespilho, F. N.; Santos, M. R. M. C.; Zucolotto, V.; Oliveira, O. N.; Silva, W. C. *J. Phys. Chem. C* **2007**, *111*, 12817−12821.
(40) Zucolotto, V.; Ferreira, M.; Cordeiro, M. R.; Constantino, C. J. L.; Balogh, D. T.; Zanatta, A. R.; Moreira, W. C.; Oliveira, O. N. Jr *J. Phys. Chem. B* **2003**, *107*, 3733−3737.
(41) Choi, J.; Rubner, M. F. *Macromolecules* **2005**, *38*, 116−124.
(42) Maldonado, S.; Stevenson, K. J. *J. Phys. Chem. B* **2004**, *108*, 11375−11383.
(43) Lampert, A.; Mark, P. *Current Injection in Solids*; Academic Press: New York, 1970.
(44) Yang, Y. C.; Pan, F.; Liu, Q.; Liu, M.; Zeng, F. *Nano Lett.* **2009**, *9*, 1636−1643.
(45) Lee, C.; Kim, I.; Choi, W.; Shin, H.; Cho, J. *Langmuir* **2009**, *25*, 4274−4278.
(46) Kim, Y.; Lee, C.; Shim, I.; Wang, D.; Cho, J. *Adv. Mater.* **2010**, *22*, 5140−5144.
(47) Chudnovskii, F. A.; Odynets, I. I.; Pergament, A. I.; Stefanovich, G. B. *J. Solid State Chem.* **1996**, *122*, 95−99.
(48) Simmons, J. G.; Verderber, R. R. *Proc. Roy. Soc. A* **1967**, *301*, 77−102.
(49) Choi, T. L.; Lee, K.-H.; Joo, W.-J.; Lee, S.; Lee, T.-W.; Chae, M. Y. *J. Am. Chem. Soc.* **2007**, *129*, 9842−9843.
(50) Guan, W.; Long, S.; Jia, R.; Liu, M. *Appl. Phys. Lett.* **2007**, *91*, 062111−062113.
(51) Liu, C.; Fan, W.; Straus, D. A.; Lei, B.; Asano, S.; Zhang, D.; Han, J.; Meyyapan, M.; Zhou, C. *J. Am. Chem. Soc.* **2004**, *126*, 7750−7751.
(52) Ko, Y.; Kim, Y.; Baek, H.; Cho, J. *ACS Nano* **2011**, *5*, 9918−9926.
(53) Onitsuka, O.; Fou, A. C.; Ferreira, M.; Hsieh, B. R.; Rubner, M. F. *J. Appl. Phys.* **1996**, *80*, 4067−4071.